Author(s): Oja, Riku & Nieminen, Risto M.

Title: Modeling charge-imbalanced NaNbO3/SrTiO3 superlattices: Lattice relaxation and metallicity

Year: 2009

Version: Final published version

Please cite the original version:

Oja, Riku & Nieminen, Risto M. 2009. Modeling charge-imbalanced NaNbO3/SrTiO3 superlattices: Lattice relaxation and metallicity. Physical Review B. Volume 80, Issue 20. 205420/1-12. ISSN 1550-235X (electronic). DOI: 10.1103/physrevb.80.205420.

Modeling charge-imbalanced $NaNbO_3/SrTiO_3$ superlattices: Lattice relaxation and metallicity

Riku Oja and Risto M. Nieminen
COMP/Department of Applied Physics, Helsinki University of Technology, P.O. Box 1100, Espoo FI-02015 TKK, Finland
(Received 31 August 2009; revised manuscript received 27 October 2009; published 19 November 2009)

The electronic and structural properties of different charge-imbalanced perovskite oxide $NaNbO_3/SrTiO_3$ superlattices are investigated with density-functional theory (local density approximation and local spin density approximation+U) methods. Metallic or insulating behavior of such a superlattice depends on the types of interfaces present: nonstoichiometric composition of a superlattice introduces holes to O p orbitals or extra electrons to Nb/Ti d orbitals. Lattice parameters, superlattice volume, and the extent of conduction electron or hole states are found to depend on interface type. The extent of the metallic state may also depend on the $NaNbO_3/SrTiO_3$ ratio. Octahedral rotations and other low-symmetry phases increase the gap between p and d orbitals but do not affect metallicity. Adding a Hubbard U to account for possible electronic correlations does not affect electron localization. Within LSDA+U, the delocalized holes align ferromagnetically.

DOI: 10.1103/PhysRevB.80.205420 PACS number(s): 73.21.Cd, 77.84.Dy, 71.28.+d, 68.65.Cd

I. INTRODUCTION

Perovskite superlattices are interesting materials for future electronics components, as they have exploitable electronic properties that cannot be achieved in bulk semiconductors. Among these are enhancement of ferroelectric polarization,[1] enhanced permittivity,[2] novel charge and magnetic ordering, and interface conductivity,[3–5] none of which are present in the constituent bulk materials. The origins of such behavior are twofold. First, lattice strain, due to different equilibrium lattice constants, affects the phase adopted by a perovskite, and often dominates the superlattice behavior. Second, a variety of electrostatic effects occur at the interfaces between layers, resulting in electronic and ionic rearrangements of the interface region.

Here we investigate superlattices consisting of alternating $NaNbO_3$ and $SrTiO_3$ layers. This combination has been selected because of the similar pseudocubic bulk lattice constants, namely, 3.905 Å for $SrTiO_3$ and 3.908 Å for $NaNbO_3$. Thus, the lattice mismatch at the interface is negligible and we may focus on other interface effects. $NaNbO_3$ and $SrTiO_3$ are interesting candidate materials for lead-free piezoelectric ceramics. Both $SrTiO_3$ and $NaNbO_3$ are simple band insulators, with gaps of 3.4 (Ref. 6) and 3.2 eV,[7] respectively. In bulk, both perovskites display complex phase transition sequences as a function of temperature, and they are very close to a ferroelectric transition when 0 K is approached.[8,9] The ground state of both perovskites is affected by ionic zero-point fluctuations. In $SrTiO_3$, this phase is tetragonal paraelectric (space group $I4/mcm$ with octahedral rotation sequence $a^0a^0c^-$ in Glazer's notation,[10] i.e., out-of-phase tilting around one axis). For $NaNbO_3$, the phase is rhombohedral ferroelectric $R3c$ or orthorhombic paraelectric (octahedral rotation $a^-a^-a^-$, i.e., out-of-phase tilts around all axes), depending on whether quantum fluctuations completely suppress ferroelectricity or not.[9]

In $NaNbO_3/SrTiO_3$ superlattices, an increase in the lattice constant and volume was observed when the number of interfaces is increased.[11] In such a superlattice, the thickness ratio of $NaNbO_3$ to $SrTiO_3$ layers was suggested to be 3:1. Additionally, decreased permittivity was observed with an increasing number of interfaces. This was assumed to be due to the interface region having different permittivity than bulk.

$NaNbO_3$ and $SrTiO_3$ are an interesting combination in that $SrTiO_3$ has nominally neutral (100) layers while the $NaNbO_3$ layers have alternating nominal charges. Charge-imbalanced interfaces are known to have rich behavior: a high-mobility electron gas has been observed in the $LaAlO_3/SrTiO_3$ interface,[12] leading to metallicity of the interface layer. Such two-dimensional (2D) electron gases have attracted much attention due to their high conductivity and possible tunability.[13] The metallicity of such a structure is determined by the superlattice layer thickness, as it depends on the energetics of charge transfer from bulk oxide to interface region. Lattice relaxation from the ideal perovskite positions has been calculated to be considerable in charge-imbalanced interfaces.[14–16]

The two possible interfaces present in our superlattice are shown in Fig. 1. To retain charge neutrality and prevent the "polar catastrophe,"[17] i.e., a divergent electric field due to an uncompensated dipole, the SrO-NbO_2 interface has an extra half an electron per unit cell compared to nominal charges and is therefore denoted n type, while the NaO-TiO_2 interface has half a hole and is denoted p type.

It is interesting to study how the presence of $SrTiO_3$ and the imposition of tetragonal or monoclinic symmetry by the superlattice affects the preferred phase of $NaNbO_3$. The nominal interface charges and dipoles will also affect the relaxation of the structure.

In this study, to investigate the properties of the (100) interface between $NaNbO_3$ and $SrTiO_3$, we present density-

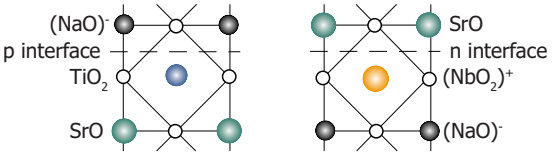

FIG. 1. (Color online) The two interface types present in a $NaNbO_3/SrTiO_3$ superlattice. In addition to the nominal charges shown, the n interface has half an electron and the p interface half a hole per interface unit cell.

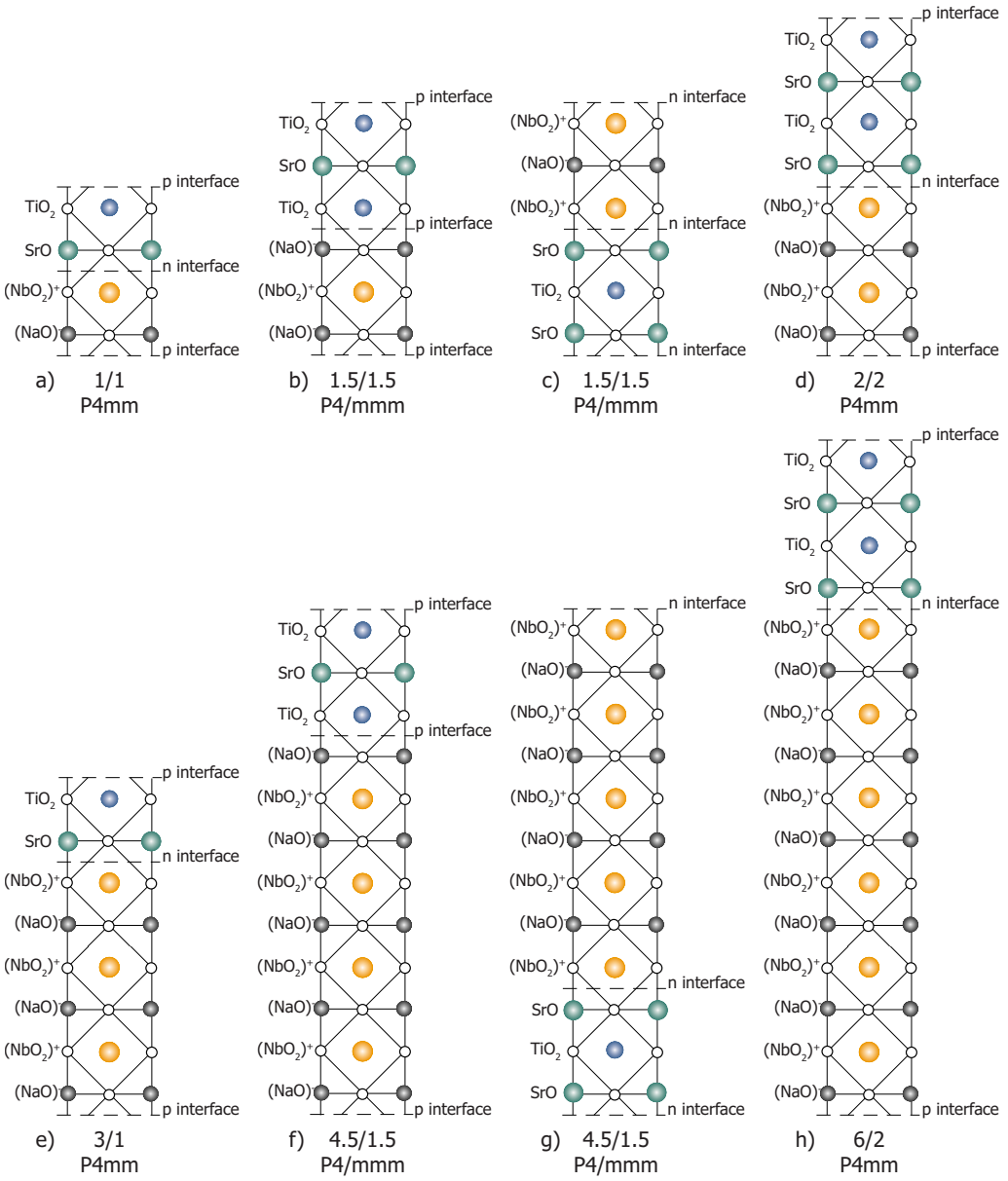

FIG. 2. (Color online) The eight considered superlattices. For each, the number of $NaNbO_3/SrTiO_3$ layers is given, along with the space group of the high-symmetry structure.

functional theory (DFT) calculations for several periodic superlattices, as shown in Fig. 2. There are four 50%/50% superlattices: (a) the 1/1 $NaNbO_3/SrTiO_3$ superlattice, which has both *n*- and *p*-type interfaces and is nominally polar, (b) the nonstoichiometric 1.5/1.5 $NaNbO_3/SrTiO_3$ superlattice, which has an extra electron due to two *n*-type interfaces, (c) the nonstoichiometric 1.5/1.5 $NaNbO_3/SrTiO_3$ superlattice, which has a hole due to two *p*-type interfaces, and (d) the 2/2 $NaNbO_3/SrTiO_3$ superlattice, which has both *n*- and *p*-type interfaces and is nominally polar. All of these structures contain equal amounts of the parent perovskites. We also performed similar calculations for the simplest possible 75%/25% $NaNbO_3/SrTiO_3$ superlattices, shown in Figs. 2(e)–2(h), to facilitate comparison with the experimental results of Ref. 11 and discern the effect of varying perovskite composition.

II. METHOD

The DFT calculations were performed using the Vienna *ab initio* simulation package (VASP).[18,19] The core states were represented using the projector augmented wave (PAW) method[20,21] and the semicore states of Na, Ti, Sr, and Nb were treated as valence electrons. The plane-wave cutoff energy throughout was 700 eV. For structural optimization, the exchange and correlation energies were described using the local-density approximation (LDA).

No in-plane strain (as imposed by a substrate) is considered, as we study the limit of a thick superlattice that is free to relax in all directions. Ionic and cell shape relaxation were performed for several unit cell volumes, to determine the minimum energy configuration within each space-group symmetry. Relaxations were stopped when the Hellmann-

Feynman forces on individual atoms were below 0.01 eV/Å. The *k*-point integration was done with the tetrahedron method with Blöchl corrections,[22] but for ionic relaxation in metallic cases, the Methfessel-Paxton method[23] was employed to obtain correct forces. The Monkhorst-Pack[24] *k*-point mesh was $6\times6\times2$ for the high-symmetry superlattices and $4\times4\times2$ for the larger doubled unit cells. For metallic superlattices, a larger *k*-point mesh $(7\times7\times3/5\times5\times3)$ with the Γ point included was applied.

For the 50%/50% superlattices, the frozen phonon method was employed to find unstable symmetry-lowering distortions of the structures: forces for all symmetrically irreducible ionic displacements in a $2\times2\times1$ supercell were calculated and the Γ- and *M*-point phonon modes with imaginary frequencies were identified. The ISOTROPY software[25] was used to identify the irreducible representations corresponding to these distortions and find the possible space groups the crystal may assume when these distortions are applied one at a time or coupled to each other. Coupling of unstable phonons must be considered to find the ground state of such a superlattice, as is evidenced by, e.g., improper ferroelectricity in a simple 1/1 $PbTiO_3/SrTiO_3$ superlattice.[26]

Correlation effects may be important in the superlattices predicted to be metallic by simple band theory: in the *n* case, we have a single electron in the *d* orbitals, while in the *p* case, a hole is present in the oxygen 2*p* orbitals. The *n* situation is similar to $LaTiO_3$ or $SrVO_3$ perovskites, where there is one electron occupying the *d* orbitals above the gap and LDA alone is known to result in erroneous prediction of metallicity, because the Mott insulating behavior is not considered.[27] Mott insulation is expected, however, only very close to d^1 occupancy,[28] which is not the case here. The *p* superlattice case resembles a $LaAlO_3/SrTiO_3$ superlattice, where correlations of oxygen 2*p* electrons may explain observed insulating behavior, localizing the hole present in these orbitals.[29] Such strongly correlated, localized electrons are not correctly described by LDA.

Therefore, in the final relaxed geometries, for comparison to LDA electron structure, a Hubbard parameter *U* describing the on-site electronic repulsion (LSDA+*U*, as implemented in VASP according to Dudarev *et al.*[30]) was added to O 2*p* and Ti/Nb 3*d*/4*d* states. Looking at the electronic energies, adding *U* will have the effect of widening the gap between valence and conduction bands closer to experimental values. However, the true band gap of a system also contains the discontinuity of exchange-correlation energy derivative with respect to particle number, which is not included in the gap between Kohn-Sham orbitals.[31] In some cases, the derivative discontinuity may be the most important factor in LDA band-gap error,[32] and it cannot be corrected with *U*. No relaxations were rerun with LSDA+*U*, as the ionic displacements under LSDA+*U* were similar to those in pure LDA, although *U* would somewhat increase the equilibrium lattice constants.

The strengths of on-site Hubbard interactions U_d and U_p were selected in the higher end of literature values, to see if any differences to LDA arise. In the rotationally invariant Dudarev[30] implementation, the only parameter is $U'=U-J$, where *U* is on-site and *J* is exchange Hartree-Fock interaction strength. The exact value of *J* will matter less than *U*, as *J* is typically in the 1 eV range and *U* several eV.

TABLE I. LDA, LSDA+*U*, and experimental values for band gaps (in eV) in the two materials.

Phase		$NaNbO_3$	$SrTiO_3$
Cubic	E_g(LDA)	1.6	1.8
Cubic	E_g(LSDA+*U*)	2.6	2.8
Unknown	E_g(expt.)	3.2[a]	3.4[b]

[a]Reference 7.
[b]Reference 6.

$U_d=8$ eV is required[29] to obtain correct Mott insulating behavior in the d^1 perovskite $LaAlO_3$, and it is also suggested to be needed in a model like ours where all *d* electrons, not just the lowest t_{2g} states, are assumed localized.[33] Therefore, we pick a high value of $U'_d=U_d-J_d=7$ eV to see if any differences to LDA arise.

Oxygen ion effective U_p values obtained by comparison to experiments on various oxides range from 3 to 8 eV, and fits to constrained LDA produce values of 3.5 to 7.5 eV.[29] In these cases, the *d* orbital of the metal ion involved is partly occupied and will partly accommodate the hole, which lowers the effective *U*. Our case, on the other hand, has the same hole occupation as the $LaAlO_3/SrTiO_3$ superlattice studied in Ref. 29, so we pick the same high value of $U'_p=U_p-J_p=6$ eV.

III. RESULTS

A. Bulk properties

The calculated LDA lattice constants in the prototype cubic phase ($Pm3m$) were 3.92 Å for $NaNbO_3$ and 3.87 Å for $SrTiO_3$. Lower than experimental lattice constants are an inherent error of LDA, independent of the material being simulated. The calculated lattice mismatch of the cubic phases is 1.4%, while experimental estimates of the cubic lattice constants give a mismatch of 0.5–1.0 %, depending on the temperature and measurement.[34,35]

Calculated band gaps for the cubic structures are listed in Table I. The gap opens between the O 2*p* and Nb/Ti 4*d*/3*d* orbitals. Adding *U* in the final geometries widens the gap closer to experimental values. The shapes of the bands are affected very little by *U*, so we can expect our LSDA+*U* results to be sensible apart from possible overemphasis of magnetization if selected *U* is too high.

Lowering the symmetry from cubic gives for both perovskites a ground state similar to the low-temperature phases reported experimentally. For $NaNbO_3$, we find the lowest-energy state to have a rhombohedral $R3c$ symmetry, with both ferroelectric displacements and octahedral rotations, doubling the size of the hexagonal unit cell. This phase has the rhombohedral lattice constants of $a=3.83$ Å and $c=3.93$ Å. For $SrTiO_3$, the lowest-energy state is a tetragonal $I4cm$ phase, which is similarly a combination of ferroelectric and antiferrodistortive modes, with lattice constants $a=3.86$ Å and $c=3.88$ Å.

Therefore the structures are the same as those found experimentally, apart from the fact that quantum suppression of

ferroelectric distortions is naturally not predicted. As our PAW potentials describe very accurately the structural properties of the bulk perovskites, they can also be expected to accurately predict the displacements in a superlattice combining these two materials.

B. Stoichiometric superlattices

The simplest considered superlattices, Figs. 2(a) and 2(d), have one or two complete unit cells of both materials. The symmetry group of such a superlattice is tetragonal *P*4*mm*, which means that there is no inversion symmetry out of plane, and all the atoms are free to relax perpendicular to the interface plane. This is because our structure has two different interfaces, *n* type and *p* type, and there is a nominal dipole perpendicular to the interface due to NbO_2 and NaO layers having different charges.

To compensate for this dipole, a large ionic as well as electronic rearrangement is expected. Indeed, if we do not relax the structure within the space group but keep the initial locations, O *p* and Nb/Ti *d* bands will overlap each other creating metallicity, an artifact of LDA and unphysical ionic locations. LDA gives similar behavior in 2/2 $LaAlO_3/SrTiO_3$ superlattices as well,[14] necessitating relaxation, although an unrelaxed configuration has been used when considering 1.5/1.5 $LaAlO_3/SrTiO_3$ superlattice electronic properties.[29] In the latter case, relaxation effects are expected to be less important as the unit cell has no dipole.

Atomic relaxation considerably changes the structure, displacing the different ions in different directions depending on their charge, to form a dipole opposite to that inherently present. The directions and approximate magnitudes of the displacements can be seen in Figs. 3(a) and 3(d). The buckling of ideally flat (100) layers may be over 10% of perovskite cell height. Similar buckling has been calculated to occur in $LaAlO_3/SrTiO_3$ superlattices.[14] The most important distortion is a rigid displacement of the oxygen octahedra with respect to the AB ion network, as a response to the interface dipole. The bulklike distortion pattern away from the interfaces is most easily seen in thicker superlattices, Figs. 3(e) and 3(h). In addition, $SrTiO_3$ cells will contract in the out-of-plane direction and $NaNbO_3$ cells will expand since the superlattice forces their in-plane lattice parameters to be same. Properties of the relaxed structures are listed in Table II.

The LDA electronic band structures for the relaxed 1/1 and 2/2 superlattices are displayed in Figs. 4 and 5. For ease of comparison, they are given in the $(\sqrt{2}\times\sqrt{2})R45°$ supercell of the cell-doubled phase reported below. First, the bandgaps of 1.1 eV for the 1/1 superlattice and 0.9 eV for the 2/2 superlattice are smaller than those predicted for the bulk materials by LDA.

Correlation effects on the band gap are considered by adding Hubbard *U* on O *p* and Nb/Ti *d* orbitals, as detailed previously. This doubles the band gaps, to 2.0 eV for the 1/1 superlattice and 1.8 eV for 2/2. As in the bulk cases, the only effect of Hubbard interaction is to open up the gap. Band structure is not otherwise significantly affected, as is expected in the case where the *p* orbitals are completely filled and *d* orbitals empty.

However, up to now we have only considered the high-symmetry superlattice in which octahedral rotations and other distortions are not present while they do occur in both $NaNbO_3$ and $SrTiO_3$ bulk at room temperature. To find out their effect on the structural and electronic properties, unstable Γ- and *M*-point phonons were identified with frozen phonon supercell calculations.

Of unstable 1/1 *P*4*mm* phonon modes, the lowest-energy structure is obtained by freezing in M_4 and Γ_5 modes simultaneously, resulting in a monoclinic *Pa* symmetry phase which has $a^-a^-c^-$ octahedral rotation sequence. Therefore, this space group also allows polarization and octahedral rotation along the in-plane diagonal, i.e., mode M_5 with order parameter $(a,0)$.

The octahedral rotation patterns for the 1/1 and 2/2 superlattices are displayed in Figs. 6(a) and 6(d). In the phases shown, no unstable phonons were found. Within the 1/1 $(\sqrt{2}\times\sqrt{2})R45°$ cell, the Nb-centered oxygen octahedron will rotate significantly around the *z* axis, the Ti centered negligibly. Around the in-plane axis, both octahedra rotate. Also, the larger 2/2 *P*4*mm* superlattice has the same unstable modes and the same ground-state *Pa* symmetry. In this case, we have two stacked Nb centered octahedra, which rotate to opposite directions around all three axes. It must be noted that the central Nb/Ti ion, not the cornering Na/Sr ion, determines the rotation tendency of each octahedron.

The patterns in whole can be compared to those of bulk $NaNbO_3$ and $SrTiO_3$: Nb centered octahedra in superlattice will rotate according to the $a^-a^-c^-$ pattern while Ti-centered octahedra rotate most closely like $a^-a^-c^0$. Interestingly, the superlattice Nb octahedron rotations override the bulk $a^-b^0c^0$ tendency of Ti octahedra and they rotate more than Ti octahedra. This is in contrast to bulk $NaNbO_3$ and $SrTiO_3$, where Ti octahedra rotate much more. Here Ti octahedron rotation pattern has to be in plane, not perpendicular to it, due to the Nb octahedra linked to them in out-of-plane direction.

Comparing the displacements in *P*4*mm* and *Pa* phases, octahedral rotations significantly decrease *z* displacements in Nb layers, which is offset by increasing buckling in the SrO layers. The lattice parameters of the *Pa* structures are listed in Table III. As expected, octahedral rotations decrease the unit-cell volume and hence the lattice parameters.

The effect of the discovered *Pa* ground state on the superlattice band structure can be seen in Fig. 7. A clear difference is seen in the bottom of the conduction band. The lowest unoccupied band is flatter in the *Pa* structures, which almost doubles the LDA band gap to 1.8 eV in 1/1 case and 1.6 eV in 2/2 case. Adding in the Hubbard *U* increases the *Pa* gap to 2.7 eV in the 1/1 superlattice and 2.2 eV in 2/2. Hence, we can expect the stoichiometric superlattices to have a band gap of same magnitude than bulk $NaNbO_3$ and $SrTiO_3$.

Such a polar and stoichiometric superlattice, with two different interfaces, might still be conducting in plane, if the distance between *n* and *p* interfaces is so large that transfer of charge will not occur.[36] This should be considered when comparing our results to experimental ones.

C. *n*- and *p*-type superlattices

Next, we take a look at the smallest possible superlattices which have two similar interfaces, Figs. 2(b) and 2(c). There-

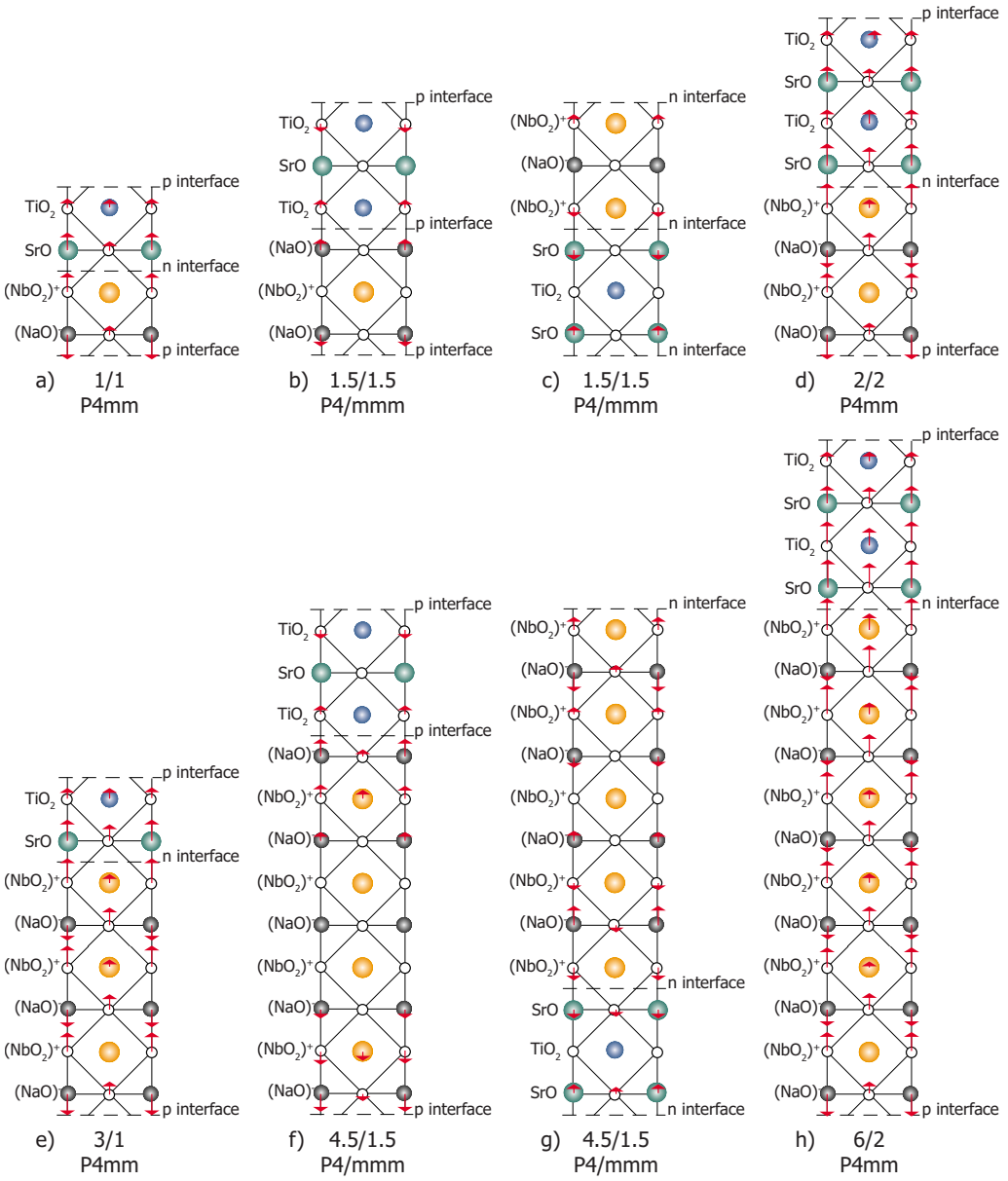

FIG. 3. (Color online) Directions and relative magnitudes of displacement, when the ionic positions are relaxed within the high-symmetry space group.

fore, they have inversion symmetry also parallel to the interface and have different numbers of different atomic layers. In both of these cases, metallic band structure is expected due to the additional electron or hole present.

The lattice parameters of these structures are listed in Table II. Unlike in the 1/1 and 2/2 superlattices, the in-plane and out-of-plane lattice parameters are seen to be almost equal. This is due to the lack of large ferroelectriclike displacements in the z direction which would stretch the unit cell. However, interface type affects the lattice parameters: the n-type superlattice ($NaNb_2Sr_2TiO_9$) has much larger lattice parameters, as it has more large Sr and Nb ions, while the p-type ($Na_2NbSrTi_2O_9$) lattice parameters are smaller due to the smaller Ti and Na ions. Hence, if one interface is energetically more favored than the other when growing a superlattice, it may increase or decrease the lattice parameter in all directions, as well as cause metallicity, by affecting the chemical composition of the superlattice.

The directions and approximate magnitudes of atomic displacements are displayed in Figs. 3(b) and 3(c). Due to the lack of an initial dipole, the displacements are much smaller than in the 1/1 and 2/2 cases. The most pronounced effect is an expansion of n type and contraction of p-type interface cells. Also, the oxygen octahedra are somewhat stretched or compressed depending on layer. However, octahedral deformation is caused by ionic variation instead of the Jahn-Teller effect: the d_{xy}, d_{xz}, and d_{yz} orbitals are all equally occupied, as detailed below.

More information can be obtained from the LDA band structures, shown in Figs. 8 and 9. The most notable difference is the location of Fermi levels in the two diagrams, meaning that the d-electron band above the gap accommo-

TABLE II. Calculated properties of the relaxed *high-symmetry* structures of the eight considered superlattices. V_{cell} is the unit-cell volume per five atoms, a the in-plane and c the perpendicular lattice constant. LDA and LDA+U indicate band-gap widths of the final structures. Experimental results from Ref. 11 are shown for comparison.

No. of NN/ST layers	Interfaces	Space group	V_{cell} (Å^3)	a (Å)	c (Å)	LDA	LDA+U
1/1	n and p	$P4mm(99)$	59	3.88	2×3.93	1.1 eV	2.0 eV
2/2	n and p	$P4mm(99)$	59	3.88	4×3.93	0.9 eV	1.8 eV
1.5/1.5	n and n	$P4/mmm(123)$	61	3.93	3×3.92	Metal	Metal
1.5/1.5	p and p	$P4/mmm(123)$	58	3.87	3×3.87	Metal	Half metal
3/1	n and p	$P4mm(99)$	60	3.89	4×3.97	1.0 eV	
6/2	n and p	$P4mm(99)$	60	3.89	6×3.97	0.9 eV	
4.5/1.5	n and n	$P4/mmm(123)$	61	3.93	6×3.94	Metal	
4.5/1.5	p and p	$P4/mmm(123)$	59	3.90	6×3.90	Metal	
4.5/1.5[a]	Unknown	Unknown	60.8	3.93	6×3.94	Insulating	
9/3[a]	Unknown	Unknown	60.7	3.93	12×3.94	Insulating	

[a]Reference 11.

dates one electron in the n case, and the O $2p$ band below the gap is missing one electron in the p case. Hence, interface metallicity is obtained. It can be seen that the addition or removal of one electron has no significant effect on band shapes, apart from bringing closer together the bands where the electron or hole is located.

Also, we present the charge density plots in the Nb/Ti-O plane for the single electron above the gap in the n case (Fig. 10) and for the hole below the gap in the p case (Fig. 11). The conduction electron in the n case (Fig. 10) occupies all Ti $3d$ and Nb $4d$ orbitals, which can be seen from the wider spread of the states around Nb and correspondingly larger density in Ti. The shape of the charge density indicates a hybrid of d_{xy}, d_{xz}, and d_{yz} orbitals, which is also seen in density of states projected to these orbitals around the Ti and Nb atoms. Therefore, no Jahn-Teller-type splitting between the d_{xy} and d_{xz}/d_{yz} energies occurs such as suggested in the $LaAlO_3/SrTiO_3$ and $LaTiO_3/SrTiO_3$ superlattices.[5,15,37]

The conduction hole in the p case (Fig. 11) occupies the hybridized oxygen orbitals of p_xp_y in the central oxygen and p_xp_z or p_yp_z in the bordering oxygens, according to the fourfold symmetry of the structure. These unoccupied electron states are those which are furthest from the positive Nb/Ti ion, as suggested by simple electrostatics. More interesting is that even in the thin $1.5/1.5p$ superlattice, the hole density is seen to be much larger in the $SrTiO_3$ than in the $NaNbO_3$ layer.

Due to the observed difference in electron localization in the p and n superlattices, charge densities were calculated for thicker 6.5/5.5 $NaNbO_3/SrTiO_3$ superlattices. The results are displayed in Fig. 12. In the p case, the hole density is approximately constant in the $SrTiO_3$ layer oxygens and goes to zero after the first NaO layer. In the n case, the electron density is maximized in the middle of the $NaNbO_3$ layer and vanishes smoothly over several perovskite unit cells. Therefore, the screening lengths of the introduced extra electrons

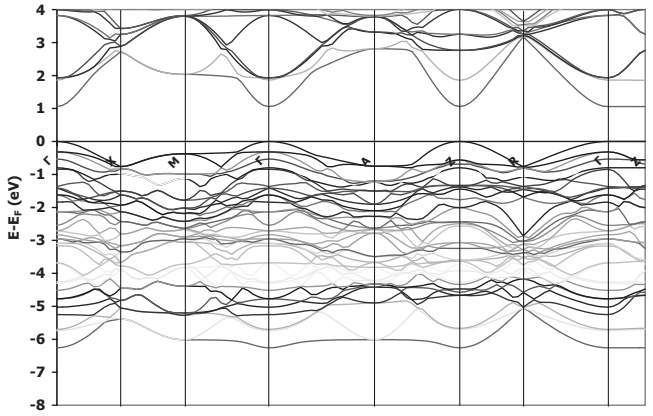

FIG. 4. LDA band structure of the relaxed 1/1 $NaNbO_3/SrTiO_3$ superlattice in the tetragonal $P4mm$ phase [$(\sqrt{2}\times\sqrt{2})R45°$ cell]. Fermi level is set at highest-occupied molecular orbital (HOMO). The tetragonal Brillouin-zone points are $\Gamma=(0,0,0)$, $X=(\frac{1}{2},0,0)$, $M=(\frac{1}{2},\frac{1}{2},0)$, $A=(\frac{1}{2},\frac{1}{2},\frac{1}{2})$, $R=(\frac{1}{2},0,\frac{1}{2})$, and $Z=(0,0,\frac{1}{2})$.

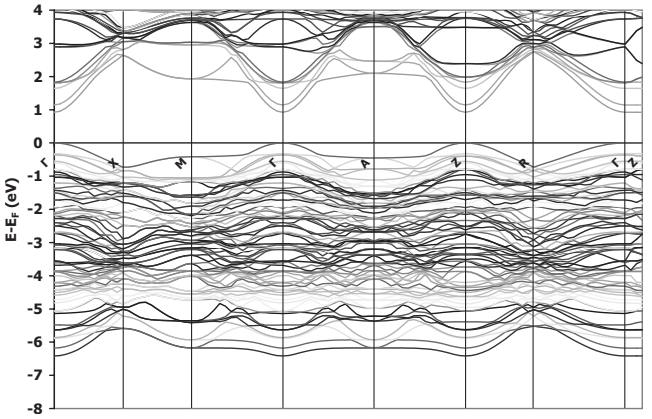

FIG. 5. LDA band structure of the relaxed 2/2 $NaNbO_3/SrTiO_3$ superlattice in the tetragonal $P4mm$ phase [$(\sqrt{2}\times\sqrt{2})R45°$ cell]. Fermi level is set at HOMO. The tetragonal Brillouin-zone points are $\Gamma=(0,0,0)$, $X=(\frac{1}{2},0,0)$, $M=(\frac{1}{2},\frac{1}{2},0)$, $A=(\frac{1}{2},\frac{1}{2},\frac{1}{2})$, $R=(\frac{1}{2},0,\frac{1}{2})$, and $Z=(0,0,\frac{1}{2})$.

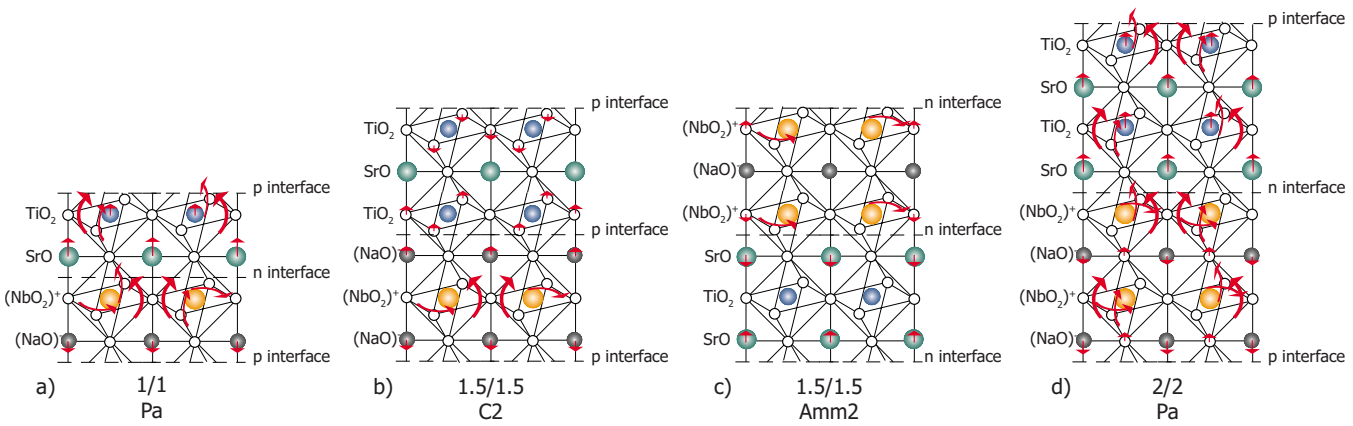

FIG. 6. (Color online) Schematic of the octahedral rotation patterns in the discovered lowest-energy structures. Displacements of 0.1 Å or more are displayed. Rotations of all four oxygens around each axis are shown by curved arrows instead.

or holes differ considerably; the holes are confined to $SrTiO_3$ layers, only affected by their immediate surroundings, while an extra electron will spread smoothly over several lattice constants and its density is maximized in the middle of $NaNbO_3$ layer.

Next, we come to the question of strong correlation effects on the electron or hole localization. Calculating the 1.5/1.5 superlattice LSDA+U electron structure on the same geometry with U'_p=6 eV and U'_d=7 eV, we obtain essentially identical charge densities. No differences can be seen in the localization of electrons in the z direction; however, as we have an odd number of electrons, ferromagnetic spin ordering is observed in LSDA+U, while simple LSDA gave vanishing magnetization. A magnetization of $1.00\mu_B$ per unit cell is obtained for the p-type superlattice. The hole depicted in Fig. 11 is, therefore, completely spin polarized and the structure is half metal in LSDA+U. In the n band structure, a magnetization of $0.80\mu_B$ per unit cell is seen, as the occupied d electron majority and minority bands overlap somewhat and metallicity is retained for both spins. This is expected, as Mott insulating behavior is known to set in only when average d orbital occupation is almost d^1 (Ref. 28).

However, for both superlattices we might obtain charge-density ordering patterns and electron localization also within the interface plane, as seen for similar $LaAlO_3/SrTiO_3$ superlattices.[29] Therefore, to rule out localized electrons, we study larger supercells which allow such patterns. Frozen phonon calculation of the n structure yields a ground state of $Amm2$ symmetry combining the M_2^+ (both Nb octahedra rotating around z in phase) and $M_5^-(a,a)$ ($SrTiO_3$ oxygen displacements similar to an $a^-b^-c^0$ pattern but limited by the mirror symmetry) phonons. The resulting rotation pattern is shown in Fig. 6(c). In the p structure only the single Nb octahedron rotates around z. Lowest energy is obtained by combining all three unstable modes, with Γ_5^- (in plane) and M_5^+ (rotation $a^-b^-c^0$) along one lattice vector, breaking the mirror plane, and M_1^+ (rotation $a^0a^0c^-$). This results in a ground state of low $C2$ symmetry and a rotation pattern displayed in Fig. 6(b). M_5^+ oxygen displacements occur in the $SrTiO_3$ layer but they are still limited by the three unit-cell supercell.

Detailed lattice constants of our ground-state structures are listed in Table III and volume reduction is once again observed as expected. It must be noted that since our supercell is three perovskite unit-cells tall, all three octahedra cannot rotate according to the out-of-phase patterns preferred by the bulk. This limits the rotation patterns available and is most probably the cause of different ground states of the two superlattices. It is likely that an actual 1.5/1.5 superlattice would have a doubled supercell in the z direction.

TABLE III. Calculated properties of the relaxed *lowest-energy* structures of the 50%/50% superlattices. Distortions refer to the irreducible representations (in parentheses the order parameters, if a distortion has several) of the Γ- and M-point phonon modes of the parent space group which have to be frozen in to obtain the ground state. V_{cell} is the unit cell volume per five atoms, a and b the in-plane and c the perpendicular lattice constants, and α the angle between lattice vectors in the monoclinic space groups. LDA and LDA+U indicate band-gap widths of the final structures. Experimental results from Ref. 11 are shown for comparison.

NN/ST	Interfaces	Distortions	Space group	V_{cell} (Å^3)	a (Å)	b (Å)	c (Å)	α (deg)	LDA	LDA+U
1/1	n and p	$\Gamma_5(a,a)\oplus M_4\oplus M_5(a,0)$	$Pa(7)$	59	$\sqrt{2}\times3.87$	$\sqrt{2}\times3.87$	2×3.89	89.7	1.8 eV	2.7 eV
2/2	n and p	$\Gamma_5(a,a)\oplus M_2\oplus M_5(a,0)$	$Pa(7)$	58	$\sqrt{2}\times3.85$	$\sqrt{2}\times3.86$	4×3.89	89.6	1.6 eV	2.2 eV
1.5/1.5	n and n	$M_5^-(a,a)\oplus M_2^+$	$Amm2(38)$	60	$\sqrt{2}\times3.89$	$\sqrt{2}\times3.89$	3×3.95	90.0	Metal	Metal
1.5/1.5	p and p	$\Gamma_5^-(a,0)\oplus M_1^+\oplus M_5^+(a,a)$	$C2(6)$	57	$\sqrt{2}\times3.84$	$\sqrt{2}\times3.84$	3×3.88	90.1	Metal	Half metal
4.5/1.5[a]	Unknown	Unknown	Unknown	60.8	3.93	3.93	6×3.94		Insulating	
9/3[a]	Unknown	Unknown	Unknown	60.7	3.93	3.93	12×3.94		Insulating	

[a]Reference 11.

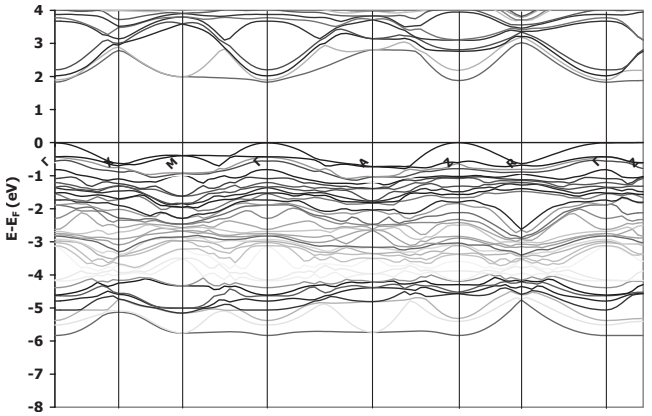

FIG. 7. LDA band structure of the relaxed 1/1 $NaNbO_3/SrTiO_3$ superlattice in the monoclinic *Pa* phase $[(\sqrt{2}\times\sqrt{2})R45°$ cell]. Fermi level is set at HOMO. The pseudotetragonal Brillouin-zone points are $\Gamma=(0,0,0)$, $X=(\frac{1}{2},0,0)$, $M=(\frac{1}{2},\frac{1}{2},0)$, $A=(\frac{1}{2},\frac{1}{2},\frac{1}{2})$, $R=(\frac{1}{2},0,\frac{1}{2})$, and $Z=(0,0,\frac{1}{2})$.

The LDA band structure of the low-symmetry phases displays similar behavior to the 1/1 superlattice, in that octahedral rotations increase the gap between *p* and *d* orbitals, but they do not affect predicted metallicity. The charge-density distributions are essentially identical to the high-symmetry phases.

Adding a Hubbard *U* further increases the gap but LSDA+*U* charge-density plots are still identical: when considering a ferromagnetic (FM) spin alignment of holes in the $(\sqrt{2}\times\sqrt{2})R45°$ *p*-type *C*2 cell or electrons in the $(\sqrt{2}\times\sqrt{2})R45°$ *n*-type *Amm*2 cell, no further localization or symmetry breaking due to *U* is observed.

An antiferromagnetic (AFM) spin alignment might require larger supercells in *xy* plane.[29] Therefore, it was calculated in a 2×2 supercell. In *n*-type superlattice, LSDA+*U* and AFM ordering breaks the degeneracy of d_{xy}, d_{xz}, and d_{yz} orbitals, and the spins mainly occupy d_{xz} states of the *Amm*2 structure. Such an orbital ordering is induced by the octahedral rotations which break the symmetry between *x* and *y*

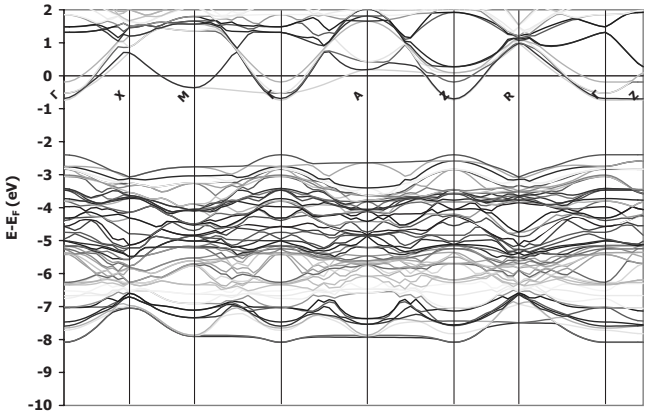

FIG. 8. LDA band structure of the relaxed 1.5/1.5 *n* $NaNbO_3/SrTiO_3$ superlattice in the tetragonal *P*4/*mmm* phase $[(\sqrt{2}\times\sqrt{2})R45°$ cell]. Fermi level is set at zero. The tetragonal Brillouin-zone points are $\Gamma=(0,0,0)$, $X=(\frac{1}{2},0,0)$, $M=(\frac{1}{2},\frac{1}{2},0)$, $A=(\frac{1}{2},\frac{1}{2},\frac{1}{2})$, $R=(\frac{1}{2},0,\frac{1}{2})$, and $Z=(0,0,\frac{1}{2})$.

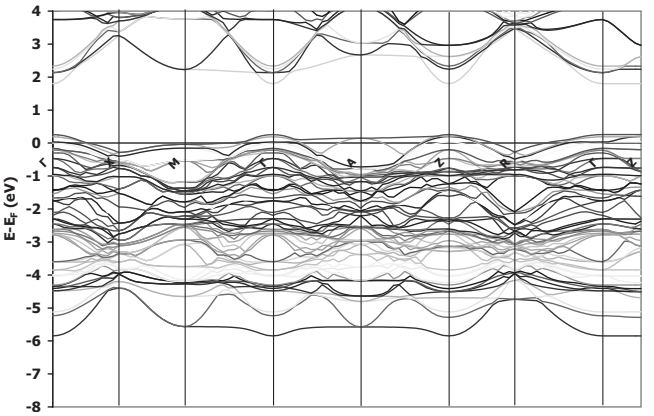

FIG. 9. LDA band structure of the relaxed 1.5/1.5 *p* $NaNbO_3/SrTiO_3$ superlattice in the tetragonal *P*4/*mmm* phase $[(\sqrt{2}\times\sqrt{2})R45°$ cell]. Fermi level is set at zero. The tetragonal Brillouin-zone points are $\Gamma=(0,0,0)$, $X=(\frac{1}{2},0,0)$, $M=(\frac{1}{2},\frac{1}{2},0)$, $A=(\frac{1}{2},\frac{1}{2},\frac{1}{2})$, $R=(\frac{1}{2},0,\frac{1}{2})$, and $Z=(0,0,\frac{1}{2})$.

directions. Still, no further localization of the extra electron occurs. Similarly, in *p*-type superlattice, the AFM solution is just as delocalized as the FM solution, although opposite spins clearly occupy different layers.

It must be noted that the *p* superlattice 2×2 supercell is ferromagnetic in LSDA+*U* while only vanishing magnetization is obtained with pure local spin density approximation. An LSDA+*U* magnetization of $4.00\mu_B$ per supercell is obtained, and the AFM solution is 0.27 eV higher in energy than FM solution. Hence, the half metallicity and ferromagnetic ordering persist for holes in *p* superlattice while the *n* superlattice FM and AFM states are approximately equal in energy.

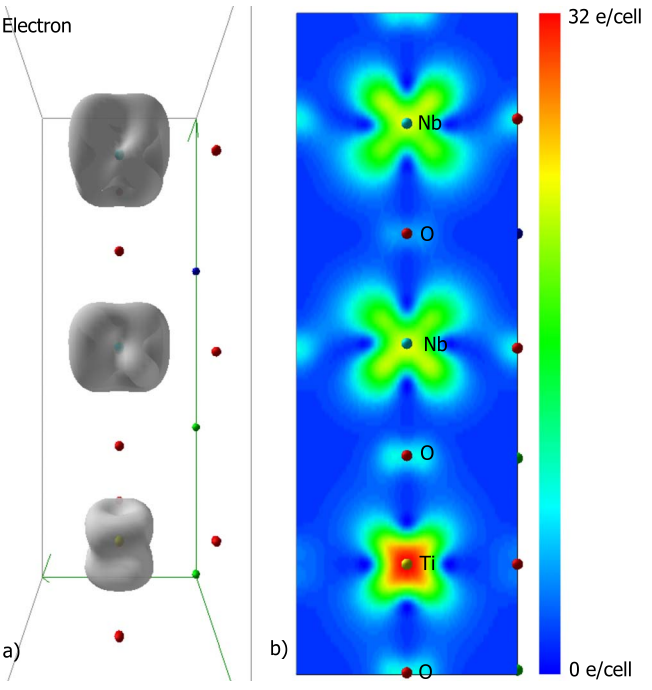

FIG. 10. (Color online) (a) Charge-density isosurfaces (at 5 e/cell) and (b) charge density plot (in logarithmic scale) for the single electron above the gap in 1.5/1.5 *n* superlattice.

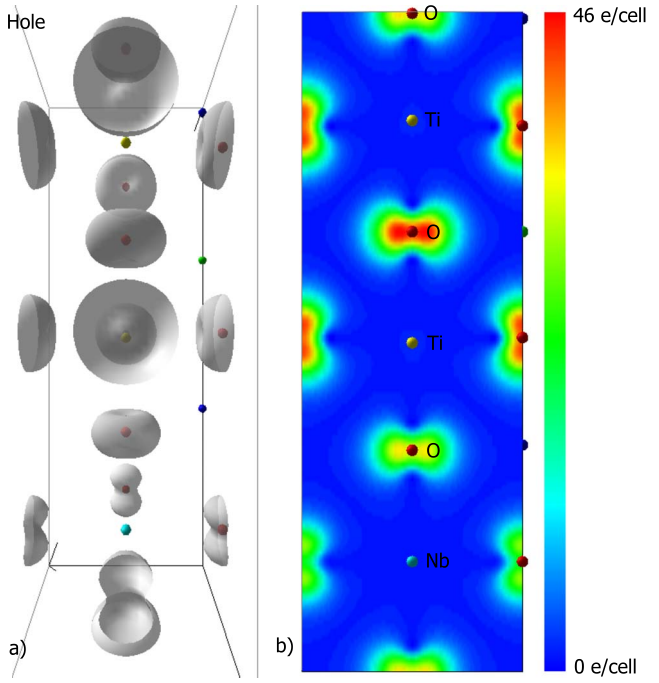

FIG. 11. (Color online) (a) Charge density isosurfaces (at 5 e/cell) and (b) charge-density plot (in logarithmic scale) for the single hole below the gap in 1.5/1.5 *p* superlattice.

D. 75% $NaNbO_3$/25% $SrTiO_3$ superlattices

Finally, we consider increasing the amount of $NaNbO_3$ layers in the superlattice to 75%. The four simplest superlattices with such a ratio are displayed in Figs. 2(e)–2(h). In such structures, a decrease in permittivity and an increase in lattice parameters, compared to a bulk mixture with the same $NaNbO_3/SrTiO_3$ ratio, were observed.[11]

The properties of the relaxed high-symmetry structures are listed in Table II. As can be observed, an increase in the number of $NaNbO_3$ layers results in corresponding increase in lattice parameters, most importantly in out-of-plane direction as the presence of a $SrTiO_3$ layer limits in-plane expansion.

Calculated lattice constants for 4.5/1.5 superlattice with *n*-type interfaces correspond to experimental results obtained for 75% $NaNbO_3$/25% $SrTiO_3$ superlattices in Ref. 11. Therefore, we suggest that observed increased lattice constants are due to nonstoichiometry of the superlattice, i.e., due to *n*-type interfaces, causing a relative increase in large Sr and Nb ions. Prevalence of *p* interfaces, on the other hand, would decrease the lattice constants to below bulk values. Layer-by-layer lattice constants (distances between atomic layers) for the *n* interface case are shown in Fig. 13. It can be seen that $NaNbO_3$ unit cells are larger than $SrTiO_3$ cells, as oxygen layer distances are increased. Na-Na distances, on the other hand, are the same as Sr-Sr distance; the interface unit cell is stretched as Sr-Na distance is considerably large. Similarly, in the *p* superlattice case, the interface cells contract.

The effect of octahedral rotations was not calculated for the 75% $NaNbO_3$/25% $SrTiO_3$ superlattices. Therefore, our LDA predictions for the lattice constants are close to experimental ones; including the rotations would result in lower lattice constants. The rotation patterns and lattice constants obtained for the smaller superlattices cannot directly be used to estimate the behavior of a 75% $NaNbO_3$/25% $SrTiO_3$ structure: a larger supercell and increased number of $NaNbO_3$ layers will result in different structures.

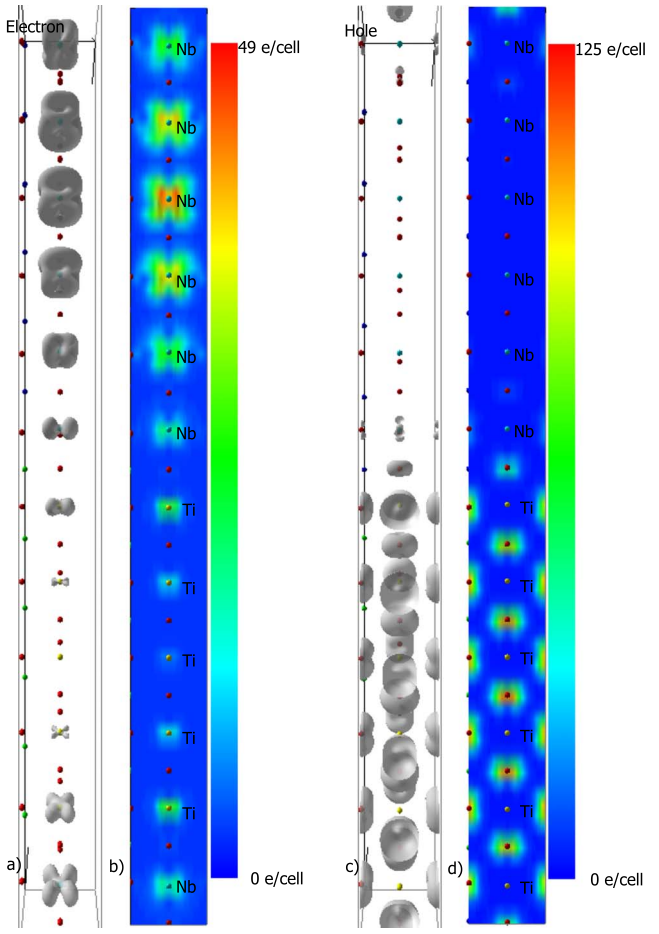

FIG. 12. (Color online) (a) Charge-density isosurfaces (at 5 e/cell) and (b) charge-density plot (in logarithmic scale) for the single electron above the gap in 6.5/5.5 *n* superlattice, and (c) charge-density isosurfaces (at 5 e/cell) and (d) charge-density plot (in logarithmic scale) for the single hole below the gap in 6.5/5.5 *p* superlattice.

As seen in Table II, the band gap or band structure were not noticeably affected by increasing the thickness of $NaNbO_3$ layer. Hence, it can be expected that our results obtained for the simplest superlattices also apply in those cases where the number of $SrTiO_3$ and $NaNbO_3$ layers are different.

However, the extent of the conducting interface state may depend on the ratio of constituent perovskites, as seen in the 75%/25% superlattice charge-density profiles plotted in Fig. 14. As expected, the conduction electron density of the *n* superlattice is largest in the middle $NaNbO_3$ layer. However, the hole density of *p* superlattice is noticeable also in $NaNbO_3$ while it is larger in $SrTiO_3$ layers. This means that the energy difference between $SrTiO_3$ and $NaNbO_3$ oxygen $2p$ orbitals is so small that hole localization depends on the amount of doping and available $SrTiO_3$ layers, and $NaNbO_3$

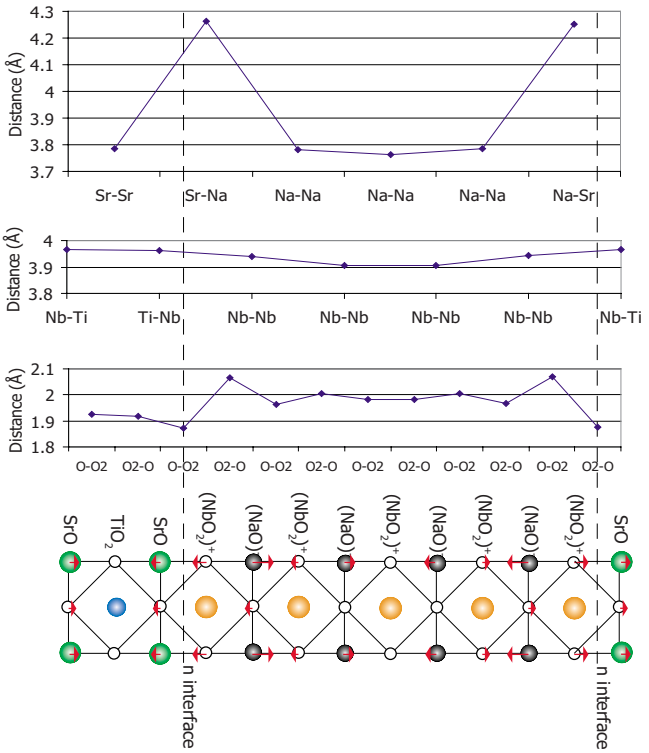

FIG. 13. (Color online) Calculated ionic distances between each layer in the 4.5/1.5 *n*-type superlattice.

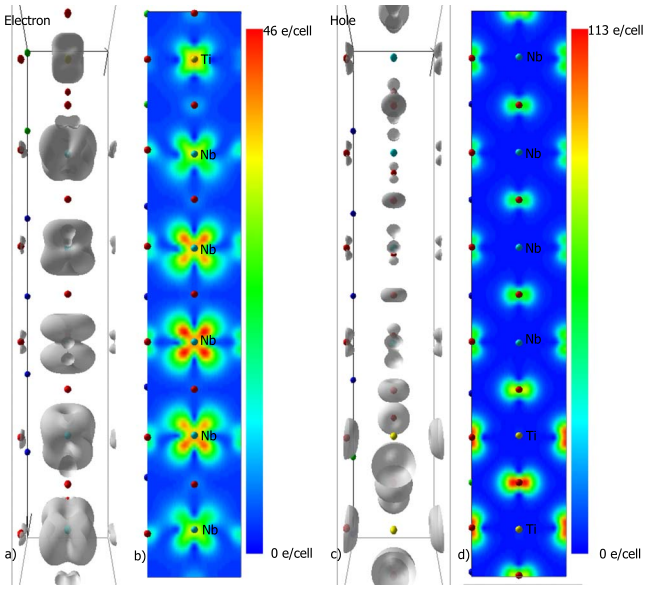

FIG. 14. (Color online) (a) Charge-density isosurfaces (at 5 e/cell) and (b) charge-density plot (in logarithmic scale) for the single electron above the gap in 4.5/1.5 *n* superlattice, and (c) charge-density isosurfaces (at 5 e/cell) and (d) charge-density plot (in logarithmic scale) for the single hole below the gap in 4.5/1.5 *p* superlattice.

orbitals will accommodate part of the hole if only a single $SrTiO_3$ layer is present.

IV. DISCUSSION AND CONCLUSIONS

In this study simple, atomically sharp $NaNbO_3/SrTiO_3$ superlattice structures were considered, assuming that at least one atomic layer of each constituent element is present in an artificially grown superlattice. Structural relaxations were performed to allow for both ionic and electronic compensation of the interface dipoles, as well as octahedral rotations in the smallest superlattices. Within LDA and LSDA+U, the relaxed stoichiometric superlattices are insulating while the *n* or *p* interfacially doped (nonstoichiometric) superlattices are metallic, as expected from simple band theory.

The results indicate that superlattice properties, including metallic or insulating behavior and lattice constant, are not determined merely by layer thicknesses. Instead, the type of the interface between the perovskites is a crucial factor. If one interface type is energetically more favored than the other, growing such a superlattice may result in metallicity and an increase or decrease in lattice constants, as the superlattice is nonstoichiometric.

Growth of lattice volume when increasing the number of interfaces was observed in Ref. 11, which would be consistent with a superlattice having more *n* than *p* interfaces. If the volume increase was caused by oxygen vacancies instead, it should not be affected by the number of interfaces and the perovskite types involved.

Insulating behavior was observed in all grown superlattices in Ref. 11. This is surprising as a superlattice with *n* interfaces should display in-plane metallicity, and also a superlattice with different interfaces could be metallic in-plane, if the interface separation is too large for charge transfer to happen. In $LaAlO_3/SrTiO_3$ superlattices, the critical interface separation was observed to be six perovskite unit cells,[36] above which in-plane conductivity of the superlattice would increase.

However, an explanation for insulating behavior are imperfections of the superlattices. A single interface cannot be expected to extend continuously in plane across a macroscopic sample, as defects are bound to exist in the superlattice. Not all polar interfaces are even energetically stable,[38] but the structures considered here are expected to exist experimentally, as electronic compensation of the interface dipoles is possible and occurs in DFT through Ti/Nb mixed valency (*n* case) and O mixed valency (*p* case). X-ray diffraction results of Ref. 11 also indicated that atomically sharp superlattices have been grown but this does not guarantee continuous interfaces across the sample.

The additional electron density in *n* superlattice calculations occupies Nb and Ti $4d/3d$ orbitals, centered on the central $NaNbO_3$ layer and diminishing over several perovskite unit cells. On the other hand, the hole density in *p* superlattices equally occupies all $SrTiO_3$ layer O $2p$ orbitals and is lower in $NaNbO_3$ layers. Whether the holes occupy $NaNbO_3$ oxygens at all depends on the amount of doping relative to the amount of $SrTiO_3$ layers available.

This behavior is different to that in similarly relaxed $LaAlO_3/SrTiO_3$ superlattices, where the holes are calculated to be delocalized and electrons localized to only Ti orbitals.[14,16,39] On the other hand, the extra *d* electron in a $LaTiO_3/SrTiO_3$ superlattice has been observed[3] to be extended over several nanometers, just as in our

$NaNbO_3/SrTiO_3$ case. It seems that the critical layer thickness, below which three-dimensional metallicity occurs, in our superlattice will be dependent on the interface type as well as the ratio of perovskite layers, i.e., number of available orbitals. Better determination of the confinement width of the 2D electron gas at a single interface would require calculations with larger superlattices[39] to discern the interfaces.

It must be noted that electron delocalization is a well-known artifact of LDA, but our results with additional Hubbard interactions (LSDA+U) show no localized charge-ordering patterns or significant differences in conduction electron or hole localization. However, LSDA+U magnetization and half metallicity of the holes is obtained even in a 2×2 supercell. Such delocalized ferromagnetic ground states have been obtained earlier for similar holes,[29] and they have been suggested to give rise to magnetic effects at interfaces between nonmagnetic oxides.[4]

Ionic displacements in the insulating superlattices may be very large, over 10% of the perovskite lattice constant, because of the polar supercell. A ferroelectriclike displacement of ions occurs throughout the structure to compensate for the dipole. No ferroelectricity is present, however, as the polar superlattice has no inversion symmetry. The metallic superlattices have smaller displacements located at the interface cells. In all superlattice types, however, lattice elongation of the $NaNbO_3$ layers is seen, in accordance with the measurements of Ref. 11. We suggest that the origin of decreased permittivity, as observed in Ref. 11, is the considerable polar distortion already present in a superlattice with a large amount of interfaces. This could limit the ionic displacements of the superlattice when subjected to an external field, although calculations of the dielectric response of our structures are needed.

ACKNOWLEDGMENTS

This work has been supported by the Academy of Finland through its Centers of Excellence Program (2006–2011) and the FinNano Program (Project No. 128229), and a grant from the Väisälä Fund of the Finnish Academy of Science and Letters. CSC (the Finnish IT Center for Science) provided the computing resources. We acknowledge useful discussions with Marina Tyunina and her co-workers, as well as Karen Johnston, Johannes Frantti and Yukari Fujioka.

[1] J. B. Neaton and K. M. Rabe, Appl. Phys. Lett. **82**, 1586 (2003).
[2] H. Tabata, H. Tanaka, and T. Kawai, Appl. Phys. Lett. **65**, 1970 (1994).
[3] A. Ohtomo, D. A. Muller, J. L. Grazul, and H. Y. Hwang, Nature (London) **419**, 378 (2002).
[4] A. Brinkman, M. Huijben, M. van Zalk, J. Huijben, U. Zeitler, J. C. Maan, W. G. van der Wiel, G. Rijnders, D. H. A. Blank, and H. Hilgenkamp, Nature Mater. **6**, 493 (2007).
[5] J.-L. Maurice, C. Carrétéro, M.-J. Casanove, K. Bouzehouane, S. Guyard, E. Larquet, and J.-P. Contour, Phys. Status Solidi A **203**, 2209 (2006).
[6] J. Kubacki, A. Molak, and E. Talik, J. Alloys Compd. **328**, 156 (2001).
[7] *Numerical Data and Functional Relationships in Science and Technology*, Landolt-Börnstein, New Series, Group III, Vol. 41, Pt. E, edited by O. Madelung, U. Rössler, and M. Schulz (Springer-Verlag, Berlin, 2000).
[8] W. Zhong and D. Vanderbilt, Phys. Rev. B **53**, 5047 (1996).
[9] S. I. Raevskaya, I. P. Raevski, S. P. Kubrin, M. S. Panchelyuga, V. G. Smotrakov, V. V. Eremkin, and S. A. Prosandeev, J. Phys.: Condens. Matter **20**, 232202 (2008).
[10] A. M. Glazer, Acta Crystallogr., Sect. B: Struct. Crystallogr. Cryst. Chem. **28**, 3384 (1972).
[11] J. Narkilahti, M. Plekh, J. Levoska, and M. Tyunina, Phys. Rev. B **79**, 014106 (2009).
[12] A. Ohtomo and H. Y. Hwang, Nature (London) **427**, 423 (2004).
[13] S. Thiel, G. Hammerl, A. Schmehl, C. W. Schneider, and J. Mannhart, Science **313**, 1942 (2006).
[14] M. S. Park, S. H. Rhim, and A. J. Freeman, Phys. Rev. B **74**, 205416 (2006).
[15] S. Okamoto, A. J. Millis, and N. A. Spaldin, Phys. Rev. Lett. **97**, 056802 (2006).
[16] Z. S. Popovic, S. Satpathy, and R. M. Martin, Phys. Rev. Lett. **101**, 256801 (2008).
[17] W. A. Harrison, E. A. Kraut, J. R. Waldrop, and R. W. Grant, Phys. Rev. B **18**, 4402 (1978).
[18] G. Kresse and J. Hafner, Phys. Rev. B **48**, 13115 (1993).
[19] G. Kresse and J. Furthmüller, Phys. Rev. B **54**, 11169 (1996).
[20] P. E. Blöchl, Phys. Rev. B **50**, 17953 (1994).
[21] G. Kresse and D. Joubert, Phys. Rev. B **59**, 1758 (1999).
[22] P. E. Blöchl, O. Jepsen, and O. K. Andersen, Phys. Rev. B **49**, 16223 (1994).
[23] M. Methfessel and A. T. Paxton, Phys. Rev. B **40**, 3616 (1989).
[24] H. J. Monkhorst and J. D. Pack, Phys. Rev. B **13**, 5188 (1976).
[25] H. T. Stokes, D. M. Hatch, and B. J. Campbell (2007), stokes.byu.edu/isotropy.html
[26] E. Bousquet, M. Dawber, N. Stucki, C. Lichtensteiger, P. Hermet, S. Gariglio, J.-M. Triscone, and P. Ghosez, Nature (London) **452**, 732 (2008).
[27] B. Amadon, F. Lechermann, A. Georges, F. Jollet, T. O. Wehling, and A. I. Lichtenstein, Phys. Rev. B **77**, 205112 (2008).
[28] Y. Tokura, Y. Taguchi, Y. Okada, Y. Fujishima, T. Arima, K. Kumagai, and Y. Iye, Phys. Rev. Lett. **70**, 2126 (1993).
[29] R. Pentcheva and W. E. Pickett, Phys. Rev. B **74**, 035112 (2006).
[30] S. L. Dudarev, G. A. Botton, S. Y. Savrasov, C. J. Humphreys, and A. P. Sutton, Phys. Rev. B **57**, 1505 (1998).
[31] J. P. Perdew and M. Levy, Phys. Rev. Lett. **51**, 1884 (1983).
[32] N. A. Lima, L. N. Oliveira, and K. Capelle, Europhys. Lett. **60**, 601 (2002).
[33] I. Solovyev, N. Hamada, and K. Terakura, Phys. Rev. B **53**, 7158 (1996).
[34] G. Shirane, R. Newnham, and R. Pepinsky, Phys. Rev. **96**, 581 (1954).

[35] *Numerical Data and Functional Relationships in Science and Technology*, Landolt-Börnstein, New Series, Group III, Vol. 3, edited by K. H. Hellwege and A. M. Hellwege (Springer-Verlag, Berlin, 1969).
[36] M. Huijben, G. Rijnders, D. H. A. Blank, S. Bals, S. van Aert, J. Verbeeck, G. van Tendeloo, A. Brinkman, and H. Hilgenkamp, Nature Mater. **5**, 556 (2006).
[37] S. Okamoto and A. J. Millis, Nature (London) **428**, 630 (2004).
[38] N. Nakagawa, H. Y. Hwang, and D. A. Muller, Nature Mater. **5**, 204 (2006).
[39] K. Janicka, J. P. Velev, and E. Y. Tsymbal, Phys. Rev. Lett. **102**, 106803 (2009).